

Temperature dependence of the characteristics of an electrohydrodynamic pump with plate-bar electrodes

Masahito Nishikawara^{1*}, Ryo Yoneda¹, Hideki Yanada¹,
Takeshi Miyakita² and Kenichiro Sawada²

¹Dept. of Mechanical Engineering,
Toyohashi University of Technology

*phone: +81-532-44-6683

*e-mail: nishikawara@me.tut.ac.jp

²Research and Development Directorate,
Japan Aerospace Exploration Agency

Abstract—When an electrohydrodynamic (EHD) pump is used as a power source to drive a refrigerant liquid, the temperature dependence of the EHD pump characteristics needs to be made clear but has hardly been investigated. Thus, in this research, the pump characteristics are measured under different temperatures ranging from 3 to 45 °C using a fluorine solvent, Vertrel™ XF (C₅H₂F₁₀) as a working fluid. The pressure developed by the EHD pump at a zero flow rate increases with decreasing temperature and the slope of pressure-flow rate characteristics is steeper with lower temperature. The numerical simulation results obtained under the assumption that the injected charge density increases with decreasing temperature agree with experimental results and reveal the effect of fluid temperature.

I. INTRODUCTION

One of the promising applications of an electrohydrodynamic (EHD) pump is as a heat transfer device. So far, heat transfer and thermal control devices whose working fluid is liquid phase, liquid-vapor two-phase, or air have been developed utilizing the EHD phenomenon, [1-16]. For liquid phase application, there are microchannel cooling systems driven by micropump integrated EHD electrodes [1], enhancement of forced convection heat transfer in a duct with disturbance induced by EHD flow [2] and a cryogenic cooling system of liquid nitrogen loop driven by an EHD pump [3, 4]. For two-phase applications, there are enhancement of pool and flow boiling heat transfer with EHD interfacial force [5, 6], two-phase fluid loop driven by EHD conduction pumping [7-9], electrohydrodynamically augmented or driven heat pipe and vapor chamber [10, 11], enhancement of condensation heat transfer in tube flow and on tube external surface with EHD interfacial force

[12, 13]. For air application, there are wheat drying by EHD flow [14] and an air cooling system of a CPU with an EHD blower [15, 16].

When an EHD pump is used as a power source to drive a refrigerant liquid, temperature dependence of the EHD pump characteristics needs to be made clear but has hardly been investigated. So, this research investigated the effect of fluid temperature on the pump characteristics using a fluid loop. The EHD flow in the pump is simulated numerically, then the effect of fluid temperature on electrostatic pumping is explored.

II. EXPERIMENTAL SETUP

A. EHD pumps

A fabricated EHD pump, as shown in Fig.1 and 2, consists of tandemly arranged two pairs of a plate electrodes placed in the center and two-square-bar electrodes mounted on the walls in a rectangular channel 1 mm high, 5 mm wide and 16 mm long. The spacing between the plate and square-bar electrodes is 0.2 mm. These electrodes, made of stainless steel, are adhered to plastic parts, and the plastic parts are inserted into a plastic casing. Two plastic tube joints with tapped and tapered holes are attached to both sides of the casing to connect a fluid loop. These plastic parts are made of VisiJet M3 Crystal (3D Systems, Inc.) and produced by a 3D printer. The total pump size is 33 mm long, 15 mm high and 19 mm wide and the mass is 11.2 g.

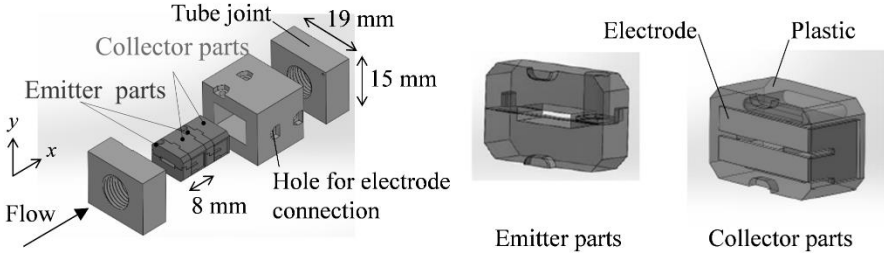


Fig. 1. Overview of the EHD pump. Electrode is made of stainless steel and the other parts are plastic. Total mass is 11.2 g and length \times height \times width is 33 mm \times 15 mm \times 19 mm. Length of a pair of emitter and collector parts is 8 mm.

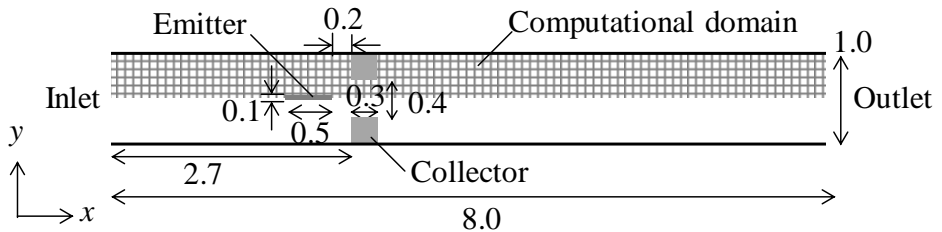


Fig. 2. Side view of the EHD pump. The electrode gap between emitter and collector is 0.2 mm. Flow channel is rectangular with a length of 8.0 mm, a height of 1.0 mm and a width of 5.0 mm. Computational domain shown as netted area is the upper half of the channel.

B. Fluid loop and experimental condition

The pump was inserted in a fluid loop system including a constant temperature plate and a regulation valve as shown in Fig. 3. The constant temperature plate consists of two aluminum plates which sandwich a main tube and two tubes where coolant flows from a chiller. A differential pressure gauge and a flowmeter were used to measure the pressure developed by the pump and volume flow rate. Two K-type thermocouples were inserted in both sides of the pump. These digital data were collected to a data logger every 5 s.

A DC voltage of -1.5 kV was applied to the plate electrode and the bar electrode was grounded. The applied polarity was adopted from the result of a preliminary experiment. The average electric field strength was 7.5 kV/mm. The pump characteristics were measured under different fluid temperatures ranging from 3 to 45 °C. The flow rate was manually controlled by the regulation valve to obtain the pressure-flow rate (P - Q) characteristics. A fluorine solvent, Vertrel™ XF ($C_5H_2F_{10}$), was used as a working fluid.

Some physical properties of Vertrel™ XF were measured under different temperature in our laboratory. The results are listed in Table 1. Density, relative permittivity and viscosity were measured using a vibrating density meter (KYOYO ELECTRONICS MANUFACTURING DA-130N), a probe consisting of two concentric cylinders (RUFUTO Model 871), and a cone-plate rotational viscometer (TOKI SANGYO RE80), respectively. The ionic mobility was determined by Walden's rule [17]. Electric conductivity was estimated by $\sigma = \sigma_{25} [1 + \alpha(T - 25)]$ [18]. α is 0.02 and σ_{25} is in catalog obtained from Du Pont-Mitsui Fluorochemicals Company, Ltd. C , C_0 , F_E , M_d , and R_e are the non-dimensional numbers that appear in the governing equations in the next section.

NUMERICAL SIMULATION

Computational domain shown as netted area in Fig. 2 is the upper half of the channel, because the computational domain is symmetrical about the centerline of the flow channel. The continuity equation (1) and the Navier–Stokes' equation (2) including Coulomb's force as the external force under a steady, laminar, and incompressible flow are solved. The

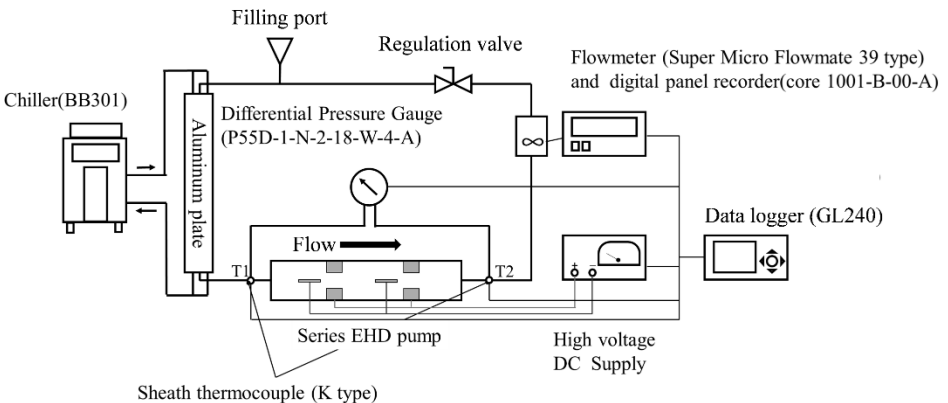


Fig. 3. Fluid loop driven by the EHD pump and measurement system. Pressure-flow rate characteristics are obtained with valve regulation.

TABLE 1: TEMPERATURE DEPENDENCE OF THE PHYSICAL PROPERTIES AND NON-DIMENSIONAL NUMBERS OF THE WORKING FLUID, VERTREL™ XF (C₂H₅F₁₀)

	3 °C	25 °C	45 °C
Density, ρ [kg/m ³]	1,640	1,580	1,520
Conductivity, σ [S/m]	1.93×10^{-8}	3.45×10^{-8}	4.83×10^{-8}
Relative permittivity, ϵ [-]	7.99	6.84	5.78
Viscosity, μ [mPa·s]	0.952	0.647	0.482
Ionic mobility, μ_+ [m ² /V·s]	3.15×10^{-8}	4.64×10^{-8}	6.22×10^{-8}
Derivative of conductivity with respect to electric field, γ [m/V]	8.30×10^{-8}	8.32×10^{-8}	8.66×10^{-8}
Coefficient of charge injection density, k [C/V·m ²]	0.0680	0.0283	0.0167
Threshold electric field strength, E_{thres} [kV/mm]	0.154	0.154	0.154
C [-]	0.23	0.11	0.078
C_0 [-]	0.23	0.33	0.40
F_E [-]	6.3×10^4	5.8×10^4	5.5×10^4
M_d [-]	2.9×10^5	5.1×10^5	7.5×10^5
R_e [-]	81	170	290

charge conservation equation for injected charges (3) and dissociated charges (4 and 5) and Gauss' law (6) are solved simultaneously. Non-dimensional forms of these equations are

$$\nabla^* \cdot \mathbf{v}^* = 0, \quad (1)$$

$$(\mathbf{v}^* \cdot \nabla^*) \mathbf{v}^* = -\nabla^* p^* + \frac{1}{R_e} \nabla^{*2} \mathbf{v}^* + M_d \left(\frac{1}{R_e} \right)^2 q_{total}^* \mathbf{E}^*, \quad (2)$$

$$\nabla^* \cdot \left(-w_{in}^* \mathbf{E}^* + w_{in}^* \mathbf{v}^* - \left(\frac{1}{F_E} \right) \nabla^* w_{in}^* \right) = 0, \quad (3)$$

$$\nabla^* \cdot \left(q^* \mathbf{E}^* + q^* \mathbf{v}^* - \left(\frac{1}{F_E} \right) \nabla^* q^* \right) = \frac{C_0^2 F(E)}{\left(1 + \frac{1}{b_r} \right)} - \left(1 + \frac{1}{b_r} \right) q^* w^*, \quad (4)$$

$$\nabla^* \cdot \left(-w^* \mathbf{E}^* + w^* \mathbf{v}^* - \left(\frac{1}{F_E} \right) \nabla^* w^* \right) = \frac{C_0^2 F(E)}{\left(1 + \frac{1}{b_r} \right)} - \left(1 + \frac{1}{b_r} \right) q^* w^*, \text{ and} \quad (5)$$

$$\nabla^{*2} \phi^* = -q_{total}^*. \quad (6)$$

Here, symbols with an asterisk are non-dimensional variables. $\mathbf{v}=(u, v)$ is the velocity vector, p is the pressure, \mathbf{E} is the electric field vector, w_{in} is the density of the negative charges injected from the negative electrode, q and w are the respective densities of the positive and negative charges generated by dissociation, and ϕ is the electric potential. The non-dimensional numbers appearing in (1-6) are listed in Table 2. b_r is mobility ratio of

TABLE 2: NON-DIMENSIONAL NUMBERS IN THE GOVERNING EQUATIONS

Symbol	Expression
b_r	$\frac{\mu_+}{\mu_-}$
C	$\frac{w_e L^2}{\varepsilon V_e}$
C_0	$\frac{\sigma L^2}{\mu_+ \varepsilon V_e}$
F_E	$\frac{\mu_+ V_e}{D_i}$
M_d	$\frac{\varepsilon V_e^2}{(\mu^2 / \rho)}$
R_e	$\frac{\mu_+ V_e}{(\mu / \rho)}$

positive and negative dissociation charges, C_0 is non-dimensional parameter in source term of dissociated charge conservation equation, F_E is ion drift number, M_d is Masuda number, and R_e is electric Reynolds number, μ_+ , μ_- are ionic mobilities of positive and negative dissociation charges, respectively, σ is the conductivity, L is characteristic length, ε is the permittivity, V_e is applied voltage, D_i is the diffusion coefficient of ions, ρ is the liquid density, μ is the viscosity, and $q_{total} = -w_{in} + q - w$. Temperature dependence of the non-dimensional numbers are listed in Table 1. This model assumes that only negative charges are injected and that they do not combine with the positive dissociation charges because the injected negative charges are in general different from the dissociated negative charges. It is assumed for simplicity that the ionic mobilities of the three carriers are the same. The diffusion coefficient was calculated from Stokes-Einstein equation. $F(E)$ is a function representing the field-enhanced dissociation effect. $F(E)$ can be expressed approximately by the following equation [19] and σ is represented by a linear approximation of E :

$$F(E) = \frac{k_d}{k_{d0}} = \left(\frac{\sigma}{\sigma_0} \right)^2 = (\gamma E + 1)^2 \quad (7)$$

Here, k_d is the dissociation constant, k_{d0} is the dissociation constant under no electric field, σ_0 is the conductivity under no electric field, and γ is the derivative of conductivity with respect to electric field. The derivative was calculated according to Onsager's theory [20] and is listed in Table 1.

It is assumed that charges are injected from the spot and its vicinity of the maximum electric field strength on the emitter electrode. Numerical simulation results of the EHD pump characteristics and EHD flows obtained using the above assumption were compared with experimental results and both results agreed relatively well [21, 22]. Therefore, the present numerical simulation was conducted using the same assumption as that used in [21, 22] and the charge injection region was limited to the upper right corner of the HV elec-

trode 0.05-mm long and high from the edge. The charge density, w_e , injected from an electrode can be given by

$$w_e = k(E_{static} - E_{thres}) \quad (8)$$

where k is the proportionality constant, E_{static} is the mean value of the electrostatic field strength at the charge-injection region, and E_{thres} is the threshold value of E_{static} below which no charge injection takes place. k is determined so that simulated pressure at a zero flow rate is fitted to the measured one [21]. Further details of the model are presented in [23].

The boundary conditions used in the numerical simulation are listed in Table 3, where n stands for the coordinate axis normal to the electrode surface. A parabolic velocity profile $U_{in}(y)$ was given at the inlet by assuming a developed laminar flow.

III. RESULTS AND DISCUSSION

The experimental results of two cycles with valve opening/closing on 45 °C of fluid temperature are shown in Fig. 4. The flow rate decreases, and the developed pressure increases with valve closing. The flow rate and pressure rapidly responses with changing valve opening and reach a plateau shortly.

P - Q characteristics on each fluid temperature are shown in Fig.5. The slope of P - Q characteristics is steeper with lower fluid temperature. The pressure developed by the EHD pump at zero flow rate increases with decreasing temperature, on the other hand, the flow rate at zero developed pressure increases with increasing temperature. The maximum developed pressure and flow rate were 480 Pa and 0.22 cm³/s, respectively, at 3 °C and were 330 Pa and 0.42 cm³/s (= 25 ml/min), respectively, at 45 °C. Flow rate increasing at higher fluid temperature is a favorable characteristic for thermal control devices because the heat

TABLE 3: BOUNDARY CONDITION

Location	Equation	Equation number
1. Inlet	$u = U_{in}(y) \quad v = 0 \quad q = 0 \quad w = 0 \quad w_{in} = 0 \quad \frac{\partial \phi}{\partial x} = 0$	(9)
2. Outlet	$\frac{\partial u}{\partial x} = 0 \quad \frac{\partial v}{\partial x} = 0 \quad \frac{\partial q}{\partial x} = 0 \quad \frac{\partial w}{\partial x} = 0 \quad \frac{\partial w_{in}}{\partial x} = 0 \quad \frac{\partial \phi}{\partial x} = 0$	(10)
3. Channel wall	$u = 0 \quad v = 0 \quad \frac{\partial q}{\partial y} = 0 \quad \frac{\partial w}{\partial y} = 0 \quad \frac{\partial w_{in}}{\partial y} = 0 \quad \frac{\partial \phi}{\partial y} = 0$	(11)
4. Symmetrical surface	$\frac{\partial u}{\partial y} = 0 \quad v = 0 \quad \frac{\partial q}{\partial y} = 0 \quad \frac{\partial w}{\partial y} = 0 \quad \frac{\partial w_{in}}{\partial y} = 0 \quad \frac{\partial \phi}{\partial y} = 0$	(12)
5. Surface of ground electrode	$u = 0 \quad v = 0 \quad \frac{\partial q}{\partial n} = 0 \quad w = 0 \quad \frac{\partial w_{in}}{\partial n} = 0 \quad \phi = 0$	(13)
6. Charge injection region	$u = 0 \quad v = 0 \quad q = 0 \quad \frac{\partial w}{\partial n} = 0 \quad w_{in} = w_e \quad \phi = V_e$	(14)
6'. Surface of HV electrode except for 6	$u = 0 \quad v = 0 \quad q = 0 \quad \frac{\partial w}{\partial n} = 0 \quad w_{in} = 0 \quad \phi = V_e$	(15)

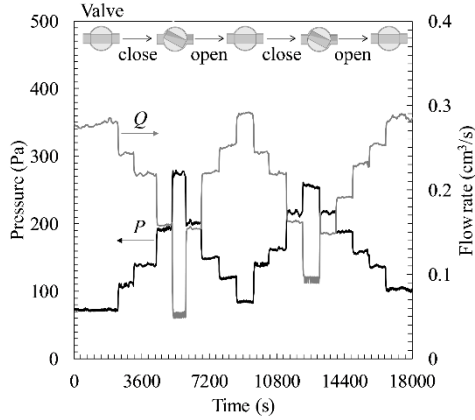


Fig. 4. Time history of developed pressure and volume flow rate on 45 °C. They are regulated with a valve from full open to close. The EHD pump could operate stably.

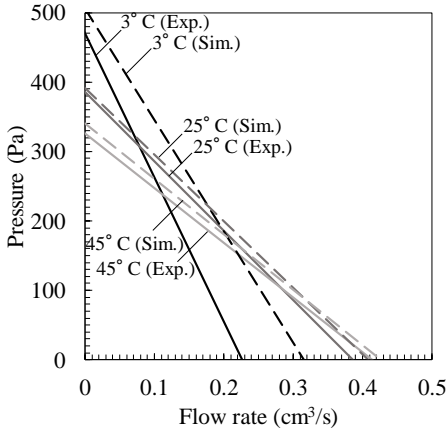


Fig. 5. P - Q characteristics on each temperature condition. Continuous lines show measured results (Exp.) depicted by least squares method. Dashed lines are simulation results (Sim.). The slope of P - Q characteristics is steeper with lower temperature.

transfer rate increases at a high heat generation rate. Pressure at a zero flow rate with a centrifugal pump, for example, used in mechanically pumped single-phase fluid loop (MPFL) for an active thermal control system (ATCS) [24] is not affected by viscosity. It is different from the characteristics of the EHD pump.

The cause that the slope of P - Q characteristics changes is attributed to the effect of viscosity. When only viscosity changed to the viscosity of 3 °C on the fluid condition of 25 °C and 45 °C, the obtained P - Q slope was almost the same as that for 3 °C. A steeper slope at a lower fluid temperature is because pressure loss in the pump is high.

To identify the cause of the pressure of the zero flow rate being high at low temperature, numerical simulations were first conducted taking only the dissociation phenomena into

consideration. Equation (3) was not solved in this simulation. The simulated charge density, velocity vector and Coulomb force vector are shown in Fig. 6. The developed pressure at zero flow rate is 39 Pa and 100 Pa on 3 °C and 45 °C, respectively. The reason high temperature shows high pressure is that dissociated charge density in the vicinity of the electrode is higher on higher fluid temperature, then the high charge density developed high Coulomb force for the right direction and induced high velocity as shown in Fig. 6. Because the non-dimensional number, C_0 is 0.23 and 0.40 at 3 °C and 45 °C, respectively, charges generated by dissociation are greater at a higher fluid temperature. As described above, temperature dependence of developed pressure when only dissociation is considered, shows a reverse trend against the measured one.

It is presumable that the injected charge density increases with decreasing fluid temperature, as a result, developed pressure at a zero flow rate is higher at a lower fluid temperature. In order to confirm the presumption, numerical simulations were conducted taking both the charge injection and dissociation phenomena into consideration. The injected charge density was determined by fitting the simulated pump pressure to the measured pressure with a zero flow rate. The simulation results obtained under the assumption that the injected charge density increases with decreasing temperature agreed with experimental results with relatively good accuracy, as shown in Fig. 5. Fig. 7 shows simulated charge density and Coulomb force distribution at a zero flow rate. The Coulomb force in the right side of emitter at 3 °C is larger than that at 45 °C, as a result, developed pressure at 3 °C is high. In addition, the place of the zero Coulomb force line at 3 °C is more upstream as compared to the place at 45 °C, so the force field where force is easily transmitted for the right direction is formed at 3 °C. This is attributed to the pressure increasing at a low fluid temperature. Non-dimensional number, C is 0.23 and 0.078 at 3 °C and 45 °C, respectively, so injected charge density, C is comparable with dissociated charge density C_0 at 3 °C. These comparable numbers lead to the formation of the Coulomb force field which can develop high pressure downstream.

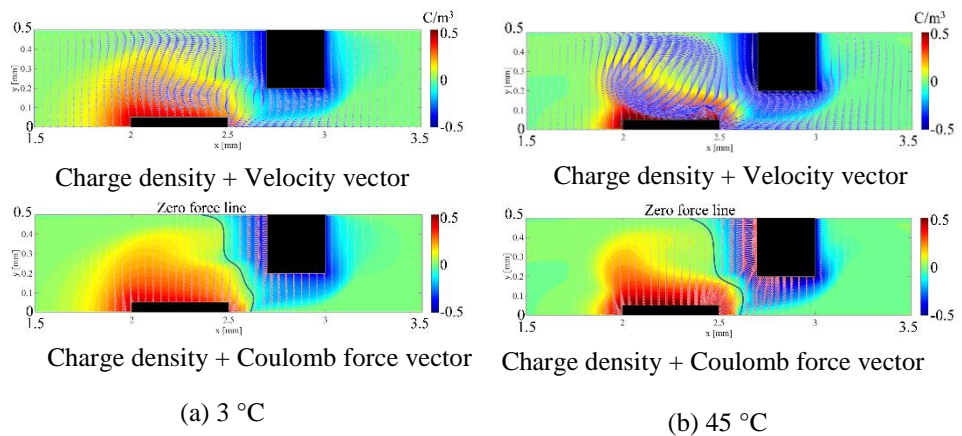


Fig. 6. Simulated charge density, velocity vector and Coulomb force vector in the pump at each temperature condition when only dissociation is considered and flow rate is zero. Charge density in the vicinity of electrodes is higher on higher fluid temperature. As a result, induced high Coulomb force leads high-speed fluid motion.

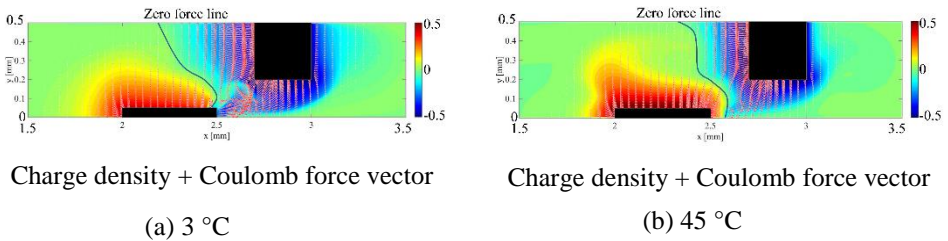


Fig. 7 Simulated charge density and Coulomb force vector in the pump on each temperature condition when both the charge injection and dissociation phenomena are considered and flow rate is zero. The simulated P - Q curve is fitted by measurement results. Higher charge density at the emitter injection region on lower fluid temperature is set in the simulation. The Coulomb force in the right side of the emitter is high and zero force line is drawn upstream on 3 °C.

IV. CONCLUSION

This paper investigated temperature dependence of the characteristics of the EHD pump with plate-bar electrodes, experimentally and numerically. The slope of P - Q characteristics is steeper with lower temperature, and the pressure at a zero flow rate is higher at lower temperature. From the numerical simulation, considering injected and dissociated charges, the reason for the latter characteristic is the temperature dependence of injected charge density from the plate emitter electrode. It was found that the effect of fluid temperature on the pumping by dissociated charge is opposite to that by injected charge. The results of the developed numerical model agreed with the measurement. The obtained knowledge contributes to fluid loop for a thermal control system using an EHD pump.

ACKNOWLEDGEMENT

This research was partially supported by JSPS KAKENHI Grant number 16K06076.

REFERENCES

- [1] V. Singhal and S. V. Garimella, "A novel valveless micropump with electrohydrodynamic enhancement for high heat flux cooling," *IEEE Transactions on Advanced Packaging*, vol. 28, pp. 216–230, May 2005.
- [2] M. Hasegawa, A. Yabe, and H. Nariai, "Numerical Analysis of Electro-hydrodynamical Enhancement Mechanism of Forced Convection Heat Transfer in Duct Flow," *Trans. Japan Soc. Mech. Eng. Ser. C*, vol. 64, pp. 1196–1201, 1998. (in Japanese)
- [3] J. Darabi and H. Wang, "Development of an electrohydrodynamic injection micropump and its potential application in pumping fluids in cryogenic cooling systems," *J. Microelectromechanical Syst.*, vol. 14, pp. 747–755, Aug. 2005.
- [4] M. Rada, A. Shooshtari, and M. M. Ohadi, "Experimental and numeral simulation of meso-pumping of liquid nitrogen-Application to cryogenic spot cooling of sensors and detectors," *Sensors and Actuators a-Physical*, vol. 148, pp. 271–279, Nov. 2008.
- [5] I. Kano and N. Okamoto, "Experimental Verification of a Prediction Model for Pool Boiling Enhanced by the Electrohydrodynamic Effect and Surface Wettability," *J. Heat Transfer*, vol. 139, pp. 084501-1-7, Aug. 2017.
- [6] J. Cotton, A. J. Robinson, M. Shoukri, and J. S. Chang, "A two-phase flow pattern map for annular channels under a DC applied voltage and the application to electrohydrodynamic convective boiling analysis," *Int. J. Heat Mass Transf.*, vol. 48, pp. 5536–5579, Dec. 2005.
- [7] S. Jeong and J. Didion, "Thermal control utilizing an electrohydrodynamic conduction pump in a two-phase loop with high heat flux source," *J. Heat Transf.*, vol. 129, pp. 1576–1583, Nov. 2007.

- [8] V. K. Patel, F. Robinson, J. Seyed-Yagoobi, and J. Didion, "Terrestrial and microgravity experimental study of microscale heat-transport device driven by electrohydrodynamic conduction pumping," *IEEE Trans. Ind. Appl.*, vol. 49, pp. 2397–2401, May 2013.
- [9] M. R. Pearson and J. Seyed-Yagoobi, "Electrohydrodynamic Conduction Driven Single- and Two-Phase Flow in Microchannels With Heat Transfer," *J. Heat Transfer*, vol. 135, pp. 101701-1-10, Oct. 2013.
- [10] B. Suman, "A steady state model and maximum heat transport capacity of an electrohydrodynamically augmented micro-grooved heat pipe," *Int. J. Heat Mass Transf.*, vol. 49, pp. 3957–3967, Oct. 2006.
- [11] M. R. Pearson and J. Seyed-Yagoobi, "Experimental Study of Linear and Radial Two-Phase Heat Transport Devices Driven by Electrohydrodynamic Conduction Pumping," *J. Heat Transfer*, vol. 137, pp. 022901-1-9, Feb. 2014.
- [12] H. Sadek, A. J. Robinson, J. S. Cotton, C. Y. Ching, and M. Shoukri, "Electrohydrodynamic enhancement of in-tube convective condensation heat transfer," *Int. J. Heat Mass Transf.*, vol. 49, pp. 1647–1657, May 2006.
- [13] K. Brand and J. Seyed-Yagoobi, "Experimental Study of Electrohydrodynamic Induction Pumping of a Dielectric Micro Liquid Film in External Horizontal Condensation Process," *J. Heat Transfer*, vol. 125, pp. 1096–1105, Dec. 2003.
- [14] W. Cao, Y. Nishiyama, and S. Koide, "Electrohydrodynamic drying characteristics of wheat using high voltage electrostatic field," *J. Food Eng.*, vol. 62, pp. 209–213, May 2004.
- [15] N. E. Jewell-Larsen, H. Ran, Y. Zhang, M. K. Schwiebert, K. A. Honer, and A. V. Mamishev, "Electrohydrodynamic (ehd) cooled laptop," presented at Annu. IEEE Semicond. Therm. Meas. Manag. Symp., San Jose, CA, March 15-19, 2009.
- [16] A. A. Ramadhan, N. Kapur, J. L. Summers, and H. M. Thompson, "Numerical development of EHD cooling systems for laptop applications," *Appl. Therm. Eng.*, vol. 139, pp. 144–156, Apr. 2018.
- [17] I. Adamczewski, "Ionization, Conductivity, and Breakdown in Dielectric Liquids" vol. 224, Taylor and Francis, London, 1969.
- [18] K. Zhou, L. Zhang, and J. Ling, "Electrical conductivity soft-sensing system based on amplitude-phase characteristics detection," *Procedia Eng.*, vol. 16, pp. 846–853, 2011.
- [19] J. K. Park, J. C. Ryu, W. K. Kim, and K. H. Kang, "Effect of Electric Field on Electrical Conductivity of Dielectric Liquids Mixed with Polar Additives: DC Conductivity," *J. Phys. Chem. B*, vol. 113, pp. 12271–12276, Sep. 2009.
- [20] L. Onsager, "Deviations from Ohm's law in weak electrolytes," *J. Chem. Phys.*, vol. 2, pp. 599–615, 1934.
- [21] H. Yanada, T. Yamada, Y. Asai, and Y. Terashita, "Measurement and numerical simulation of ion drag pump characteristics," *J. Fluid Sci. Technol.*, vol. 5, pp. 617–631, 2010.
- [22] K. D. Tran, Y. Kojima, and H. Yanada, "Measurement and Numerical Simulation of Flow and Electric Fields in Charge Injection Type of Electrostatic Oil Filter," *Trans. JAPAN FLUID POWER Syst. Soc.*, vol. 40, pp. 8–15, 2009.
- [23] M. Nishikawara, H. Yanada, and K. Shomura, "Synergy between injection and dissociation mechanisms in electrohydrodynamic pumps modeled numerically," *J. Electrostat.*, vol. 93, no. March, pp. 137–145, 2018.
- [24] A. D. Paris, P. Bhandari and G. C. Birur, "High Temperature Mechanically Pumped Fluid Loop for Space Applications – Working Fluid Selection," presented at 34th International Conference on Environmental Systems, Colorado Springs, July 2004, 2004-01-2415.